Original Article

MOLECULAR METABOLISM

A novel peroxisome proliferator-activated receptor gamma ligand improves insulin sensitivity and promotes browning of white adipose tissue in obese mice

Dan Wu [1,4], Venkateswararao Eeda [1,4], Ram Babu Undi [2], Shivani Mann [3], Michael Stout [3], Hui-Ying Lim [2], Weidong Wang [1,*]

ABSTRACT

Objective: Nuclear receptor Peroxisome Proliferator-Activated Receptor γ (PPARγ) is a promising target for the treatment of type 2 diabetes. The antidiabetic drug thiazolidinediones (TZDs) are potent insulin sensitizers as full agonists of PPARγ, but cause unwanted side effects. Recent discoveries have shown that TZDs improve insulin sensitivity by blocking PPARγ phosphorylation at S273, which decouples the full agonism-associated side effects. PPARγ ligands that act through the blockage of PPARγ phosphorylation but lack the full agonist activity would be expected to improve insulin sensitivity without TZD-associated side effects, however, chemicals that carry such traits and bind to PPARγ with high-affinity are lacking. Moreover, TZDs are known to promote white-to-brown adipocyte conversion and energy expenditure and appear to require their full agonism on PPARγ for this activity. It is unknown whether a partial or non-TZD agonist of PPARγ is capable of promoting browning effect. In this study, we developed a novel non-TZD partial agonist of PPARγ and investigated its function on insulin sensitivity and white-to-brown conversion and energy expenditure in diet-induced obese mice.

Methods: A novel indole-based chemical W095E was designed via medicinal chemistry and tested for PPARγ binding and activity and for the effect on PPARγ phosphorylation. Diet-induced obese mice were administered with W095E for 4 weeks. Insulin sensitivity, glucose tolerance, body weight, fat tissue weight, adipocyte size, morphology, energy expenditure, and expression levels of genes involved in PPARγ activity, thermogenesis/browning, and TZD-related side effects were evaluated.

Results: W095E binds to PPARγ with high affinity and acts as a PPARγ partial agonist. W095E inhibits PPARγ phosphorylation and regulates PPARγ phosphorylation-dependent genes. W095E ameliorates insulin resistance and glucose tolerance in mice of diet-induced obesity, with minimal TZD use-associated side effects. We found that W095E promotes white-to-brown adipocyte conversion and energy expenditure and hence protects against diet-induced obesity. W095E decreases the size of adipocytes and suppresses adipose tissue inflammation. W095E also suppresses obesity-associated liver steatosis.

Conclusions: W095E improves insulin sensitivity and glucose homeostasis and promotes browning and energy expenditure by acting as a novel PPARγ phosphorylation inhibitor/partial agonist. Our findings suggest the potential of this compound or its derivative for the therapeutic treatment of insulin resistance and obesity.

Keywords Insulin resistance; Type 2 diabetes; Obesity; PPARγ; PPARγ agonist; White-to-brown conversion

1. INTRODUCTION

The nuclear receptor peroxisome proliferator-activated receptor γ (PPARγ) plays an important role in the regulation of insulin sensitivity, glucose and lipid homeostasis, and adipogenesis. It is an important therapeutic target for insulin resistance and diabetes treatment. The commonly prescribed anti-diabetic thiazolidinedione (TZD) drugs such as rosiglitazone (Rosi) act as full agonists of PPARγ to improve insulin sensitization [1]. However, TZD drugs are associated with a number of serious side effects including water retention, adiposity, weight gain, and congestive heart failure, which are believed to be caused by the full PPARγ agonism of TZDs, thereby severely hindering their clinical

[1]Department of Medicine, Division of Endocrinology, USA [2]Department of Physiology, Harold Hamm Diabetes Center, The University of Oklahoma Health Science Center, 941 Stanton L. Young Boulevard, Oklahoma City, OK 73104, USA [3]Aging & Metabolism Program, Oklahoma Medical Research Foundation, Oklahoma City, OK, USA

[4] These authors contributed equally.

*Corresponding author. University of Oklahoma Health Sciences Center, 941 Stanton L. Young Blvd., Biomedical Sciences Education Building, Oklahoma City, USA. E-mail: weidong-wang@ouhsc.edu (W. Wang).

Received August 7, 2021 • Revision received October 18, 2021 • Accepted October 20, 2021 • Available online 25 October 2021

https://doi.org/10.1016/j.molmet.2021.101363

use. PPARγ agonists that maintain insulin sensitizing effect but are devoid of TZD-related side effects would be ideal for the treatment of insulin resistance.

Recent studies indicate that the insulin sensitizing effect of TZDs is mediated by their inhibition of PPARγ phosphorylation at S273, independent of their full agonism on PPARγ [2]. In obesity, PPARγ is phosphorylated at S273 by obesity-activated protein kinases cyclin-dependent kinase 5 (CDK5) and extracellular signal-regulated kinase (ERK) [2,3]. Phosphorylation of PPARγ at S273 induces the dysregulation of a number of genes critical for insulin sensitivity, such as insulin-sensitizing adipokine adiponectin, leading to insulin resistance [2]. TZDs inhibit the CDK5- or ERK-induced phosphorylation of PPARγ at S273 [2,4], thereby reversing insulin resistance in obesity. The inhibitory activity on S273 phosphorylation by TZDs is independent of the TZD-associated deleterious side effects, thus revealing the blockade of S273 dephosphorylation as a critical means of decoupling the insulin sensitizing effect from the full agonism-associated side effects [2]. Several small molecule PPARγ ligands were recently reported to inhibit PPARγ S273 phosphorylation and harbor insulin sensitizing and anti-diabetic activity but are spared of TZD-associated side effects [4,5]. However, these compounds are of low potency [4,5].

PPARγ ligand TZDs are also known to induce the conversion of energy-storing white adipocytes into energy-burning brown-like beige or brite adipocytes in white adipose tissues (WAT) [6–8], a process commonly referred as browning. It was observed that only TZDs, but none of the partial agonists tested, are capable of promoting the browning effect, which led to the interpretation that full agonism of PPARγ is required for browning [7]. It is therefore unknown whether a PPARγ partial agonist but with the ability to inhibit PPARγ phosphorylation is capable of inducing the browning effect.

In this study, we developed a novel non-TZD indole derivative WO95E that possesses highly potent PPARγ binding affinity and inhibits PPARγ S273 phosphorylation but with mild PPARγ transactivation activity. WO95E increases insulin sensitivity with no apparent adiposity, water retention, weight gain, or heart hypertrophy in diet-induced obese (DIO) mice. WO95E protects the mice against high fat diet-induced obesity and increases the white-to-brown adipocyte conversion and energy expenditure. In all, our study provides first demonstration that this class of compounds act as potent therapeutic agents in insulin sensitization and browning remodeling of WAT and could serve as a promising lead for further development for the treatment of T2D and obesity.

2. MATERIALS AND METHODS

2.1. Chemicals, cell culture reagents, and plasmids

The 3T3-L1 mouse fibroblasts and HEK-293 (ATCC, Manassas, VA, USA) were maintained at 37 °C in a 5% CO_2, humidified atmosphere. The cells were cultured in Dulbecco's modified Eagle's medium (DMEM), containing 4.5 g/L glucose with 10% fetal bovine serum (FBS; HyClone, Logan, UT, USA). PolarScreen™ PPARγ-Competitor Assay Kit was purchased from Thermo Fisher Scientific (Waltham, US). Bright-Glo™ Luciferase Assay System was purchased from Promega (Madison, US). Oil Red O was purchased from Alfa Aesar (Haverhill, MA, USA). Rosiglitazone was purchased from Sigma. UHC1 and WO95E were synthesized in-house. DMSO was used as solvent and as vehicle control at 0.1% in cell-based assays. Plasmids pBabe bleo human PPARγ2 (#11439) and PPRE X3-TK-luc (#1015) were acquired from Addgene.

2.2. In vitro competition binding assay

The in vitro competition binding assays was performed using PolarScreen™ PPARγ-Competitor Assay Kit according to the manufacturer's instructions. Briefly, compounds at 2-fold titration serial concentrations were incubated with GST-tagged PPARγ ligand-binding domain (LBD, 34 nM) and Fluormone PPAR Green tracer (9 nM) for 4 h in the dark at room temperature in a black 384-well assay plate (Corning Glass catalog no. 677). The fluorescence polarization value (mP) was measured at 485 nm (excitation) and at 535 nm (emission) using a microplate reader.

2.3. In silico docking simulations

The docking simulation was performed using the AutoDock Vina program. The crystal structure of PPARγ LBD (PDB ID: 5GTO) was used for the docking simulation and subsequent structural analysis. The grid dimensions for PPARγ LBD protein was 44 × 44 × 44 grid points with spacing 0.375 Å between the grid points and centered on the ligand for protein (−27.376, 18.813, 2.589 coordinates). A compound was docked in the binding pocket site using the highest accuracy mode of docking.

2.4. PPARγ transactivation reporter assay

HEK-293 cells were seeded overnight, co-transfected with plasmids expressing human PPARγ2 and 3xPPRE-luc (both from Addgene) followed by incubation for 16 h, and then re-seeded in a 384-well plate and incubated for 24 h. Compounds were added and then incubated another 24 h. Luciferase activity was analyzed in each well using Bright-Glo Luciferase kit (Promega).

2.5. Adipocyte differentiation

3T3-L1 preadipocytes were differentiated as previously described [9]. In brief, cells at around 60%—70% confluence were induced for differentiation with differentiation medium (DMEM containing 10% FBS, 1 μg/ml insulin, 1 μM dexamethasone, and 0.5 mM IBMX) for 48 h in the presence or absence of compounds and were then exposed in maintenance medium (1 μg/ml insulin in 10% FBS/DMEM) containing compounds. The medium was renewed every 2 days for total 8 days of differentiation when the cells became differentiated and lipid droplets were apparent.

For primary preadipocyte differentiation, isolation of primary preadipocytes was performed as previously described [10]. Briefly, fat depots were digested in PBS containing collagenase D (1.5U/ml) at 37 °C for 40—45 min. The primary cells were filtered through 70 μm cell strainer and centrifuge at 700 g to collect stromal vascular fraction (SVF). The SVF cell pellets were plated on collagen coated plates. Adipocyte differentiation was induced by treating confluent cells with differentiation medium (DMEM containing 10%FBS, 1 μg/ml insulin, 1 μM dexamethasone, and 0.5 mM IBMX). Two days later, the medium was changed to maintenance medium as described above for 3T3-L1 cells. The cells were cultured in the presence or absence of WO95E.

2.6. Oil Red O staining

Differentiated adipocytes were rinsed with phosphate-buffered saline (PBS) and fixed with 4% formaldehyde for 30 min. After removal of the formaldehyde, the cells were washed with PBS three times. 0.3% Oil Red O () staining solution was added to each well for 1 h incubation at 37 °C followed by washing with PBS three times. Staining of the lipid droplets were photographed using an inverted microscope (ECLIPSE TS100-F; Nikon).

2.7. Animal study

C57BL/6 J male mice were obtained from Jackson laboratory (Bar Harbor, ME) and maintained on a 12 h light (6:00 a.m. to 6:00 p.m.)–12 h dark (6:00 p.m. to 6:00 a.m.) cycle at an ambient temperature of 22 ± 1 °C. All animals had access to diet and water ad libitum. All procedures involving animals were approved by the Institutional Animal Care and Use Committee of the University of Oklahoma Health Science Center. All experiments were performed with age-matched male mice. The mice were fed a high-fat diet (HFD) (60% kcal fat, Bio-Serv, NJ, USA) starting from the age of 6 weeks until the study ends. At the 8-week HFD, mice were randomly divided into two groups and were administered daily with either vehicle (10% DMSO, 5% tween-20) or WO95E (15 mg/kg of body weight) for 4 weeks through the route of intraperitoneal injection. Food intake was determined manually by measuring the amount of input food and subtracting the amount of the food remaining in the food hopper and the crumbs on the bedding of the cage each day for three days during the 4th week of the treatment. Packed cell volume (PCV) was measured with blood drawn from tail on a LW Scientific E8 centrifuge (LW Scientific, Lawrenceville, Georgia, USA) microhematocrit centrifuge at the end of study. For all other measurements, the blood was drawn at the time of euthanization.

2.8. Glucose tolerance test and insulin tolerance test

Intraperitoneal glucose tolerance test (ipGTT) was performed after 6-h fasting. Blood glucose levels were measured at 0, 15, 30, 60, and 120 min glucometer (OneTouch Ultra 2 Meter) after an intraperitoneal administration of glucose at dose of 1.5 g/kg body weight. Intraperitoneal insulin tolerance test (ipITT) was performed after 6 h fasting. Blood glucose levels were measured at 0, 15, 30, 60, and 120 min after an intraperitoneal administration of human insulin at dose of 1.2 IU/kg body weight.

2.9. Biochemical analysis

Serum insulin (ALPCO, NH, USA), serum cholesterol TG (Cayman Chem., MI, USA) and FFAs (Bioassay system, CA, USA) were determined by ELISA.

2.10. Body composition assessment

Body lean and fat composition was determined by EchoMRI test.

2.11. Indirect calorimetry measurements

The mice were individually housed in chambers of a promethion core monitoring system (Sable Systems, Las Vegas, NV, USA). After a 1-day acclimation period, their oxygen consumption and carbon dioxide production were measured for the next three consecutive days. The respiratory exchange ratio and energy expenditure were calculated using standard equations.

2.12. Histology and immunohistochemistry

Liver, heart, bone, and adipose tissues were dissected and immediately fixed in 4% paraformaldehyde (Sigma–Aldrich), paraffin embedded, and stained with hematoxylin and eosin. For Immunofluorescence staining, the eWAT and iWAT paraffin sections were incubated with primary antibody (rabbit polyclonal to F4/80 [1:500, Cat#: 70,076], Cell Signaling Technology) overnight at 4 °C after deparaffinization. The slides were washed thrice with PBS with 0.2% Triton and then incubated in secondary antibody, Alexa 488 anti-rabbit (1:500, Jackson ImmunoResearch, PA) for 1.5 h at room temperature. Tissue sections were imaged on the Olympus Fluoview 1000 laser-scanning confocal microscope (Center Valley, PA).

2.13. RNA extraction and qRT-PCR

Total RNA (2 μg) was isolated from tissues or cells using TRIzol reagents (Life Technologies) and reverse transcribed using oligo d(T) primers (New England Biosystems) and SuperScript IV reverse transcription kit (Applied Biosystems). qPCR was performed in a CFX96 Touch Real-Time PCR detection system using SYBR Green mix (Applied Biosystems). The amplification program was as follows: initial denaturation at 95 °C for 15 min, followed by 40 cycles of 95 °C for 15 s, 60 °C for 1 min, and 40 °C for 30 s. Relative mRNA expression was determined by the $\Delta\Delta$Ct method normalized to TBP mRNA. The sequences of primers used in this study are found in Supplemental Table 1.

2.14. Western blotting

Proteins were extracted with RIPA buffer containing protease and phosphatase inhibitors (Thermo) and then centrifuged for 10 min at 10,000 *g*. A 30 μg sample of protein was separated on a 10% SDS polyacrylamide gel and transferred to polyvinylidene-fluoride membrane for 1 h at 4 °C at 40 V. The membrane was blocked in TBS (10 mm Tris–HCl, pH 7.4, 150 mm NaCl) containing 5% non-fat dry milk for 1 h at room temperature and was probed with primary antibodies, followed by the appropriate HRP-conjugated secondary antibodies (Anti-rabbit IgG, #7074, or Anti-mouse IgG, #7076, 1:5000 Cell Signaling Technology). The primary antibodies used were: anti-Ser-273 PPARγ (bs-4888 R, Bioss Antibodies), anti-PPARγ antibody (sc-271,392, Santa Cruz Biotechnology), anti-UCP1 (14670 S, Cell Signaling Technology, Beverly, MA, USA).

2.15. Synthesis of WO95E (see Scheme 1)

Reagents and solvents were obtained from commercial suppliers and were used without further purification. Reactions using air- or moisture sensitive reagents were performed under an atmosphere of Argon or Nitrogen. Reactions were monitored by TLC. Flash chromatography was performed with 230–400 mesh silica gel, and NMR spectra were measured on Bruker 400 MHz spectrometers. Chemical shifts are reported in ppm in the indicated solvent with TMS as an internal standard. Data are reported in the form: chemical shift (multiplicity, coupling constants, and integration). Multiplicities are recorded by the following abbreviations: s, singlet; d, doublet; t, triplet; q, quartet; m, multiplet; br, broad. Analytical HPLC and ESI-MS analyses were performed using either Agilent or Krats MS 80 mass spectrometer. The tested compounds were evaluated on the Agilent HPLC systems and determined to be ≥ 95% pure.

General procedure: Amino acid coupling. To a mixture of the 1-((2'-(tert-butoxycarbonyl)-[1,1′-biphenyl]-4-yl)methyl)-2,3-dimethyl-1H-indole-5-carboxylic acid (1 equivalents) in DCM was added DIEA (2.5 equivalents) and HATU (1 equivalents). The mixture was stirred for 5 min, and the 3-(aminomethyl)phenol (1 equivalents) was added. The reaction mixture was stirred at room temperature for 30 min. The

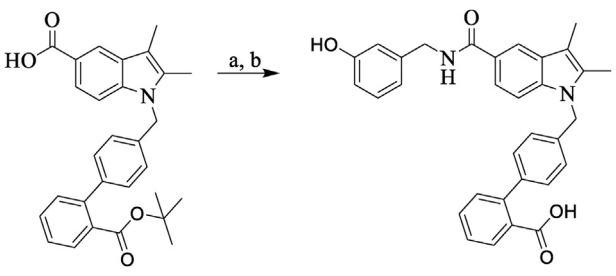

Scheme 1: Reagents and conditions: (a) HATU, DIPEA, DCM at rt; (b) TFA/DCM at ambient temperature.

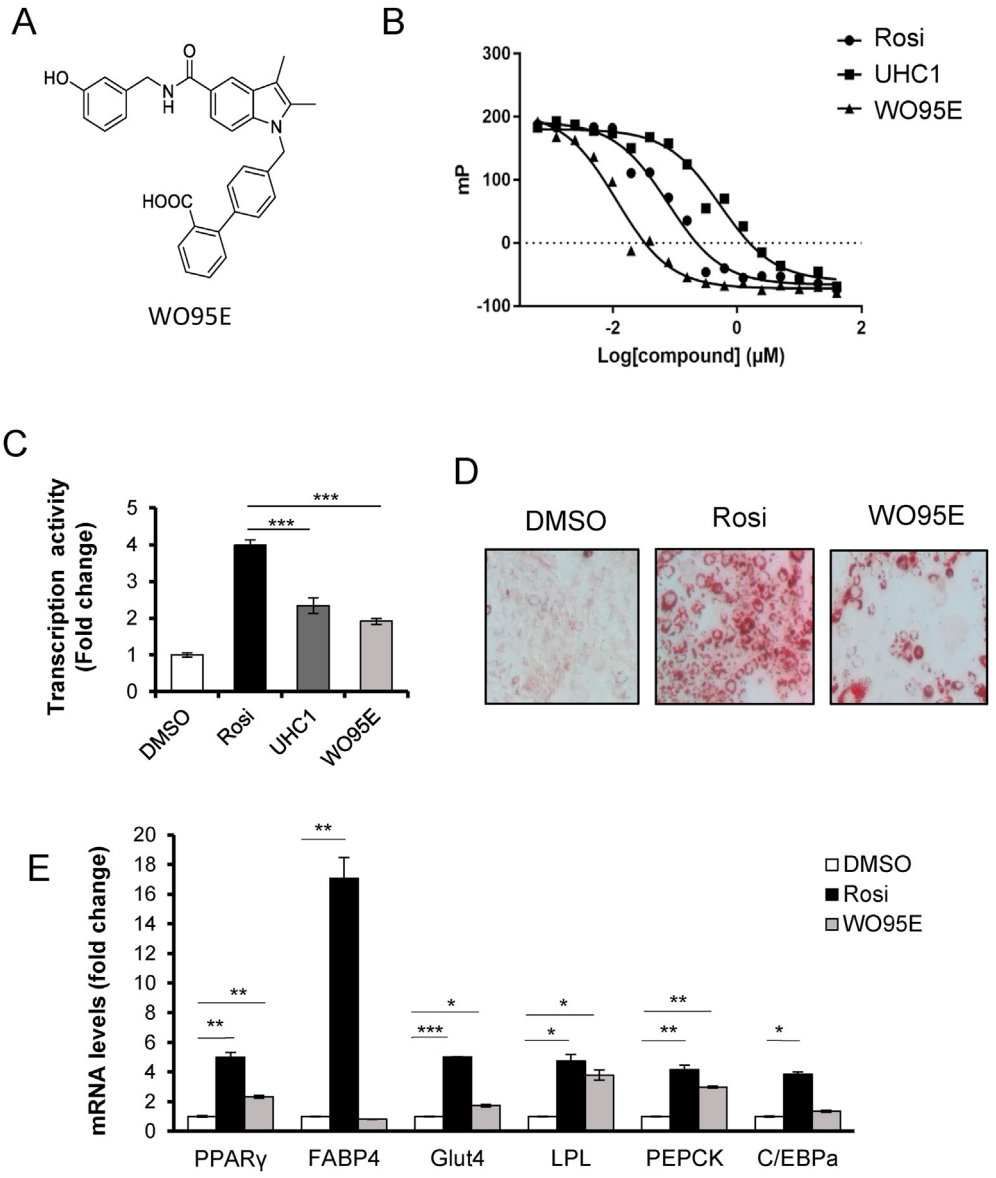

Figure 1: WO95E is a high affinity partial agonist of PPARγ. (A). Chemical structure of WO95E. (B). Binding affinity of WO95E to the ligand binding domain of PPARγ in in vitro competition binding assay. Fluorescence polarization value (mP) was measured at 485 nm (excitation) and at 535 nm (emission). The data shown are representative of 3 independent experiments. (C). Transactivation activity of compounds in HEK293 cells transfected with PPARγ2 and 3x PPRE-luc reporter. Transactivation activity was presented as fold change with that of Rosi designated as 1. The data shown are representative of 3 independent experiments. (D). Oil Red O staining in 3T3-L1 cells differentiated with differentiation media in the presence of compounds at 10 μM. (E). Relative mRNA expression levels of adipogenic genes in 3T3-L1 differentiated with differentiation media in the presence of compounds at 10 μM by qRT-PCT. The results are expressed as fold change and are representative of 3 independent experiments. Data are mean ± SEM. *P < 0.05, **P < 0.01, and ***P < 0.001.

completion of the reaction was monitored by TLC. The solvent was removed *in vacuo* to obtain the crude, which was purified by flash chromatography to provide tert-butyl 4'-((5-((3-hydroxybenzyl)carbamoyl)-2,3-dimethyl-1H-indol-1-yl)methyl)-[1,1′-biphenyl]-2-carboxylate.

Deprotection. TFA was added to solution of tert-butyl 4'-((5-((3-hydroxybenzyl)carbamoyl)-2,3-dimethyl-1H-indol-1-yl)methyl)-[1,1′-biphenyl]-2-carboxylate in DCM at room temperature. The reaction mixture was stirred at room temperature for 30 min. The completion of the reaction was monitored by TLC. The solvent was removed to obtain the crude which was purified by Flash chromatography was performed with 230–400 mesh silica gel to obtain 4'-((5-((3-hydroxybenzyl) carbamoyl)-2,3-dimethyl-1H-indol-1-yl)methyl)-[1,1′-biphenyl]-2-carboxylic acid.

WO95E: 4'-((5-((3-hydroxybenzyl)carbamoyl)-2,3-dimethyl-1H-indol-1-yl)methyl)-[1,1′-biphenyl]-2-carboxylic acid. ^{1}H NMR (DMSO-d_6, 400 MHz) δ: 9.27 (s, 1H), 8.81 (t, J = 5.7 Hz, 1H), 8.11 (s, 1H), 7.66 (m, 2H), 7.45 (m, 3H), 7.31 (d, J = 7.5 Hz, 1H), 7.24 (d, J = 7.4 Hz, 2H), 7.09 (t, J = 7.8 Hz, 1H), 6.99 (d, J = 7.6 Hz, 2H), 6.74 (m, 2H), 6.60 (d, J = 7.9 Hz, 1H), 5.46 (s, 2H), 4.42 (d, J = 5.6 Hz, 2H),

2.31 (s, 3H), 2.26 (s, 3H). ^{13}C NMR (100 MHz, DMSO-d_6) δ: 168.5, 166.0, 156.2, 140.5, 139.3, 138.6, 136.5, 136.1, 132.9, 129.5, 129.2, 128.0, 127.8, 127.4, 124.8, 123.9, 119.0, 116.6, 116.5, 112.8, 112.4, 107.6, 106.1, 44.4, 8.9, 7.6.

2.16. Statistical analysis

All data are presented as mean ± SEM of the indicated number of replicates. Data were analyzed using the unpaired two-tailed Student's t-test and $p < 0.05$ was considered statistically significant. For energy expenditure experiments, the data were analyzed for group effect (ANOVA) along with the mass and interaction effects as necessary (generalized linear model, GLM) [11].

3. RESULTS

3.1. Identification and characterization of a novel PPARγ partial agonist WO95E

Indole derivatives such as SR1664 and UHC1 were recently identified as synthetic ligands of PPARγ [4,5]. Although both compounds exhibited anti-diabetic activity without causing side effects associated with TZD use, they suffered from poor PPARγ binding affinity and pharmacokinetic properties [4,5]. We synthesized a series of indole-based analogs and investigated one analog WO95E (Figure 1A and Figure S1) as a promising PPARγ ligand. First, we assessed the binding affinity of WO95E to PPARγ by performing an in vitro competition binding assay using purified PPARγ ligand binding domain (LBD). We found that WO95E directly binds to PPARγ in a dose-dependent manner with a half-maximum inhibitory concentration (IC_{50}) of ~11 nmol/l (Figure 1B), which is approximately 70-fold lower than that of UHC1 [5], indicative of WO95E being a potent synthetic ligand of PPARγ.

We next determined the effect of WO95E on the transactivation activity of PPARγ. PPARγ acts as a transcription factor to activate the expression of its target genes by binding to the PPAR-responsive element (PRE) in their promoters. To determine the effect of WO95E on PPARγ transactivation activity, we transfected HEK293 cells with plasmids expressing PPARγ and 3XPRE-Luciferase reporter in the presence of WO95E. As shown in Figure 1C, compared to the full agonist TZD drug Rosi which markedly activated the reporter, WO95E increased the reporter activity only weakly, at ~15% and 33% of potency as Rosi and UHC1, respectively. We noted that although it was originally reported as a non-agonist PPARγ ligand [5], UHC1 activated the reporter at approximately 45% of potency as Rosi. Together, these results indicate that WO95E acts as a PPARγ partial agonist, displaying a much higher PPARγ binding affinity than indole derivatives SR1664 and UHC1 [4,5] and minimal PPARγ transactivation activity.

We then investigated the effect of WO95E on PPARγ function. As PPARγ is the master regulator of adipogenesis, we used a cell-based adipocyte differentiation assay to determine whether WO95E affects this process. PPARγ activity is essential for 3T3-L1 mouse embryonic fibroblast cells to differentiate into adipocytes. When 3T3-L1 cells were incubated with the differentiation media, as expected, addition of Rosi markedly induced the differentiation of adipocytes, as indicated by the widespread presence of lipid droplets with positive Oil Red O staining (an indication of adipocyte formation) compared to little or no Oil Red O staining in the presence of DMSO control (Figure 1D). WO95E treatment only marginally increased Oil Red O staining level (Figure 1D), indicative of its minimal effect on adipogenesis, thus corroborating the notion that WO95E is a partial agonist of PPARγ. We investigated the impact of WO95E on the expression of genes responsible for adipogenesis. PPARγ regulates the expression level of various adipogenic genes. Rosi treatment of differentiated 3T3-L1 pre-adipocytes significantly upregulated the mRNA levels of adipogenic genes PPARγ, FABP4, Glut4, PEPCK, and C/EBPa (Figure 1E). In contrast, in line with the weak effect of WO95E on adipocyte differentiation, WO95E only minimally or moderately increased the mRNA levels of these PPARγ-dependent adipogenic genes (Figure 1E).

3.2. WO95E inhibits PPARγ phosphorylation and regulates PPARγ phosphorylation-dependent genes

Indole derivatives SR1664 and UHC1 were previously shown to inhibit PPARγ phosphorylation at S273 [4,5]. As PPARγ de-phosphorylation at S273 is known to be critical for PPARγ-mediated insulin sensitivity [2], we investigated whether WO95E inhibits PPARγ phosphorylation at S273. Like Rosi and UHC1, WO95E significantly inhibited the S273 phosphorylation of PPARγ in 3T3-L1 differentiated adipocytes, using a PPARγ phospho-S273-specific antibody (Figure 2A and B). As PPARγ S273 phosphorylation is associated with the repression of a set of genes that are believed to be responsible for insulin sensitivity [2], we examined the effect of WO95E on the S273 phosphorylation-repressed genes. Our results showed that WO95E treatment led to the upregulation of the mRNA levels of a number of the PPARγ phosphorylation-dependent genes, including *adiponectin*, *cycp2f2*, *Ddx-17*, *Rarres2*, and *Selenbp1* (Figure 2C). Together, our data indicate that WO95E inhibits PPARγ phosphorylation at S273 and upregulates the PPARγ phosphorylation-dependent genes.

It was recently reported that PPARγ ligands such as SR1664 and UHC1 inhibit PPARγ S273 phosphorylation by binding to a noncanonical alternative binding pocket (ABP, which contains S273) of PPARγ, which blocks the PPARγ S273 phosphorylation from CDK5 [12–14]. We used an *in silico* docking modeling method (Autodock) to simulate WO95E's mode of binding to PPARγ. Our simulation suggests that WO95E does not bind to the canonical PPARγ ligand-binding pocket (LBP) containing H3, H3-4 loop, H11 and H12, which full agonist Rosi binds [15]; instead, WO95E binds to the ABP comprising H2′-H3, β-sheet, and the Ω loop (Figure 2D). Our modeling predicts that WO95E binding shifts the position of S273 (Figure 2E), which could explain its suppression of S273 phosphorylation. To exclude the possibility that WO95E binds to the canonical LBP of PPARγ, we employed a potent PPARγ antagonist GW9662, which binds and forms the irreversible covalent bond with the canonical PPARγ LBP (IC_{50} 3.3 nM) [16]. GW9662 largely eliminated the ability of the full agonist Rosi to activate the 3xPPRE reporter (Figure 2F and H), consistent with the prediction that Rosi is incapable of binding to the canonical PPARγ LBP in the presence of GW9662 [16]. In contrast, WO95E retained its moderate ability to activate the reporter with GW9662 co-treatment (Figure 2G and H), suggesting that WO95E binds PPARγ via an alternative site.

3.3. WO95E improves glucose tolerance and insulin sensitivity in diet-induced obese mice

We next interrogated whether WO95E improves insulin sensitivity in diet-induced obesity (DIO) mice with established insulin resistance. For this, we treated DIO mice with WO95E or vehicle via intraperitoneal injection once daily for 4 weeks. We observed that WO95E treatment significantly improved glucose tolerance with lower peak glucose level and decreased AUC (area under the curve) in response to a bolus of exogenous glucose compared to their vehicle-treated counterpart (Figure 3A–A′). Insulin sensitivity was also enhanced in DIO mice treated with WO95E (Figure 3B–B′). We found that DIO mice treated with WO95E exhibited markedly decreased fasting and refeeding plasma levels of insulin (Figure 3C), indicative of increased insulin sensitivity in the WO95E-treated mice. Similar trend in insulin levels

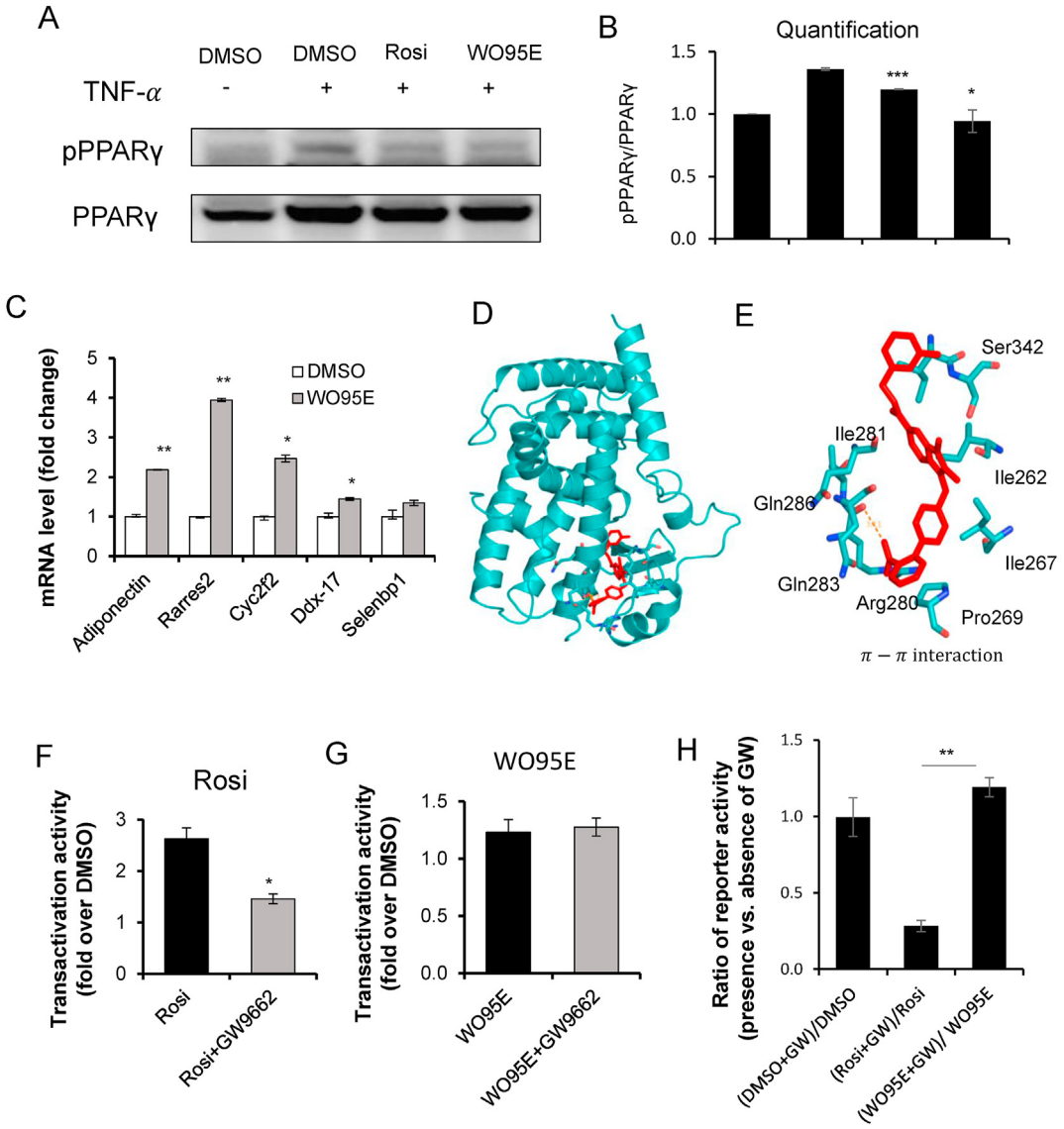

Figure 2: WO95E inhibits PPARγ S273 phosphorylation. (A). Phosphorylation of PPARγ S273 in 3T3-L1 differentiated adipocytes treated with TNFα 10 ng/ml for 1 h in the presence of compounds at 10 μM pSer273 of PPARγ was detected by Western blotting using PPARγ pSer273-specific antibody. The data shown are representative of 3 independent experiments. (B). Quantification of Phosphorylation of PPARγ S273. Data are the mean ± SEM. *P < 0.05, and ***P < 0.001 compared to DMSO control in the presence of TNFα. (C). Relative mRNA expression levels of pSer273-associated genes in 3T3-L1 differentiated with differentiation media in the presence of compounds at 10 μM by qRT-PCT. The results are expressed as fold change and are representative of 3 independent experiments. Data are mean ± SEM. *P < 0.05, **P < 0.01, and ***P < 0.001. (D). Docking simulation of the PPARγ LBD:WO95E complex. WO95E is in red. (E). Schematic representation of atomic interaction between PPARγ LBD and WO95E. Hydrogen bonds are shown in brown dashed lines with donor-acceptance distances in angstroms. (F—G). Transactivation activity of compounds in HEK293 cells transfected with PPARγ2 and 3x PPRE-luc reporter, in the presence and absence of GW9662 (5 μM). Both Rosi (F) and WO95E (G) were tested at 10 μM. Transactivation activity was presented as fold change with that of DMSO as 1. The data shown are representative of 3 independent experiments. Data are the mean ± SEM. *P < 0.05. (H). Transactivation activities shown in (F—G) were plotted as ratio of a compound in the presence of GW9662 over that in the absence of GW9662. Data are expressed as mean ± SEM. **P < 0.01 compared to DMSO control group.

was observed in mice following an exogenous bolus of glucose (Figure 3D). Collectively, these data indicate that WO95E improves insulin sensitivity and glucose disposal in DIO mice. We also observed that WO95E decreased the serum level of free fatty acid (Figure 3E), whereas total serum cholesterol showed downward trend but did not reach statistically significant (Figure 3F) and triglyceride level was unchanged (Figure S2).

We next investigated whether the improvement of insulin sensitivity in WO95E-treated DIO mice correlates with its effect on PPARγ phosphorylation at S273 in adipose tissues. First, we assessed the phosphorylation status of adipose tissues from DIO mice treated with WO95E or vehicle. As shown in Figure 3G, WO95E treatment markedly inhibited PPARγ phosphorylation in inguinal white adipose tissue (iWAT), as indicated by probing with a PPARγ phospho-S273-specific antibody. Similar results were obtained in epididymal white adipose tissue (eWAT) (Figure 3H). We examined the effect of WO95E on the expression of S273 phosphorylation-dependent genes. Our results showed that the mRNA levels of genes including *Adiponectin*, *Adipsin*, *selenbp1*, *Car3, Ddx-17, Acyl*, *Rarres2*, and, *Cidec*, which are known to be repressed by PPARγ phosphorylation, were up-

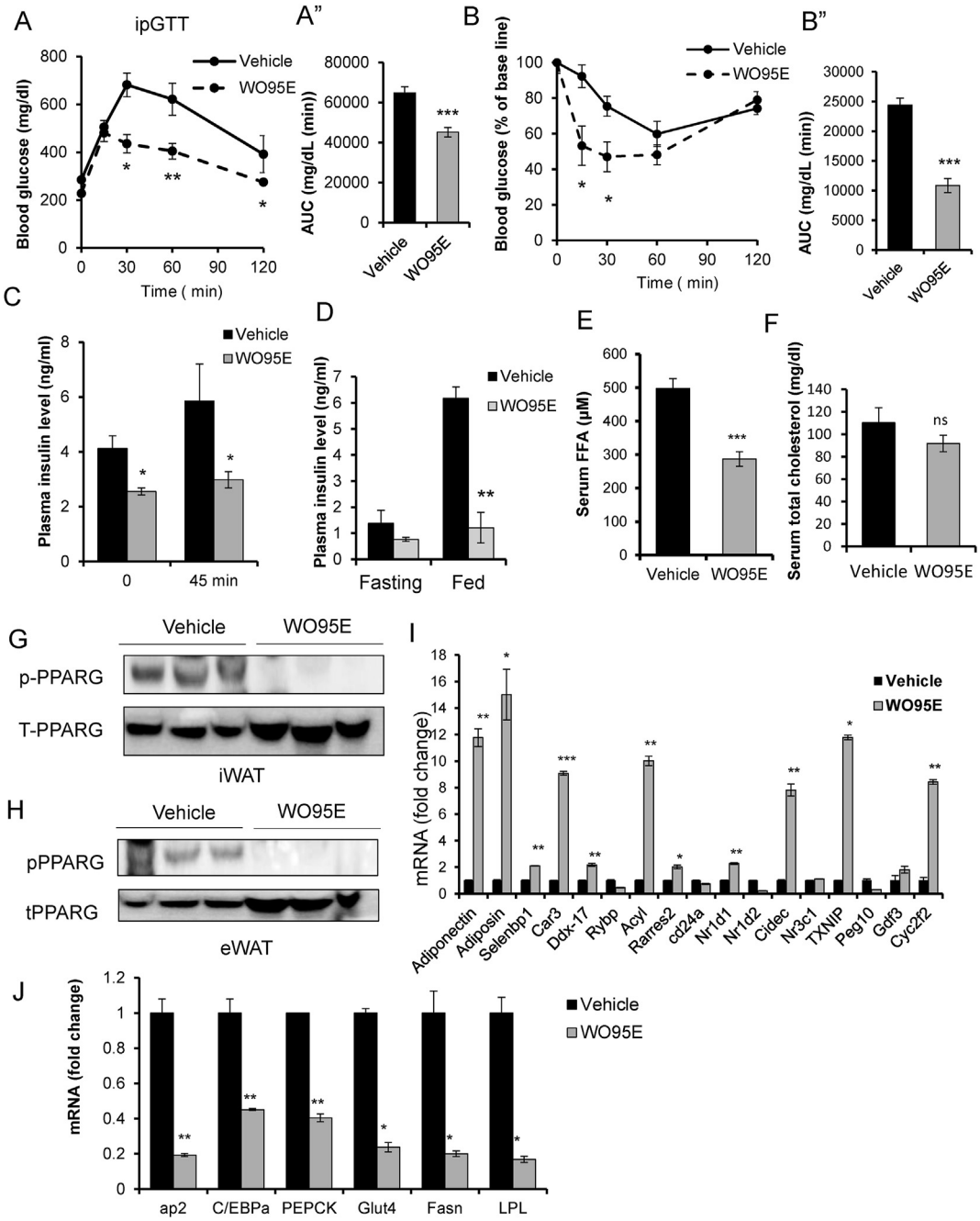

Figure 3: WO95E improves glucose tolerance and insulin sensitivity in DIO mice. (A—A′). Glucose tolerance test performed for mice treated with WO95E (n = 8) or vehicle (n = 7) for 2 weeks. Blood glucose levels (A) measured at indicated time points after intraperitoneal injection of glucose (1.5 g/kg body weight) following 6-h fasting and the AUC (area under the curve, A′). (B—B′). Insulin tolerance test performed for mice treated with WO95E (n = 8) or vehicle (n = 7) for 2.5 weeks. Blood glucose levels (B) normalized to basal level at indicated time points after intraperitoneal injection of insulin (1.2 IU/kg body weight) following 6-h fasting and the AUC (area under the curve, B′). C. Plasma insulin levels at indicated time points after intraperitoneal injection of glucose (1.5 g/kg body weight) following 6-h fasting. D. Plasma insulin levels after overnight fasting and 3-hour refeeding. E. Serum free fatty acid level. F. Serum total cholesterol level. G-H. Phosphorylation status of PPARγ protein at S273 in iWAT (G) and in eWAT (H) determined by Western blotting. The data shown are representative of 3 independent experiments. I. mRNA levels of known PPARγ phosphorylation-dependent genes determined by qRT-PCR. J. mRNA levels of adipogenic and lipogenic genes determined by qRT-PCR. The results are expressed as fold change and are representative of 3 independent experiments. Data are expressed as mean ± SEM. # P < 0.1, *P < 0.05, **P < 0.01, and ***P < 0.001.

regulated by WO95E treatment (Figure 3I), whereas genes involved in lipogenesis or adipogenesis were inhibited (Figure 3J) in eWAT. Similar to that seen in cultured adipocytes, WO95E suppresses PPARγ phosphorylation and up-regulates the PPARγ-phosphorylation-repressed genes in adipose tissue.

3.4. WO95E protects against diet-induced obesity and increases energy expenditure

In addition to insulin sensitization, we observed that WO95E also protected against diet-induced obesity. As shown in Figure 4A, while vehicle-treated mice continue to increase body weight under high fat diet (HFD),

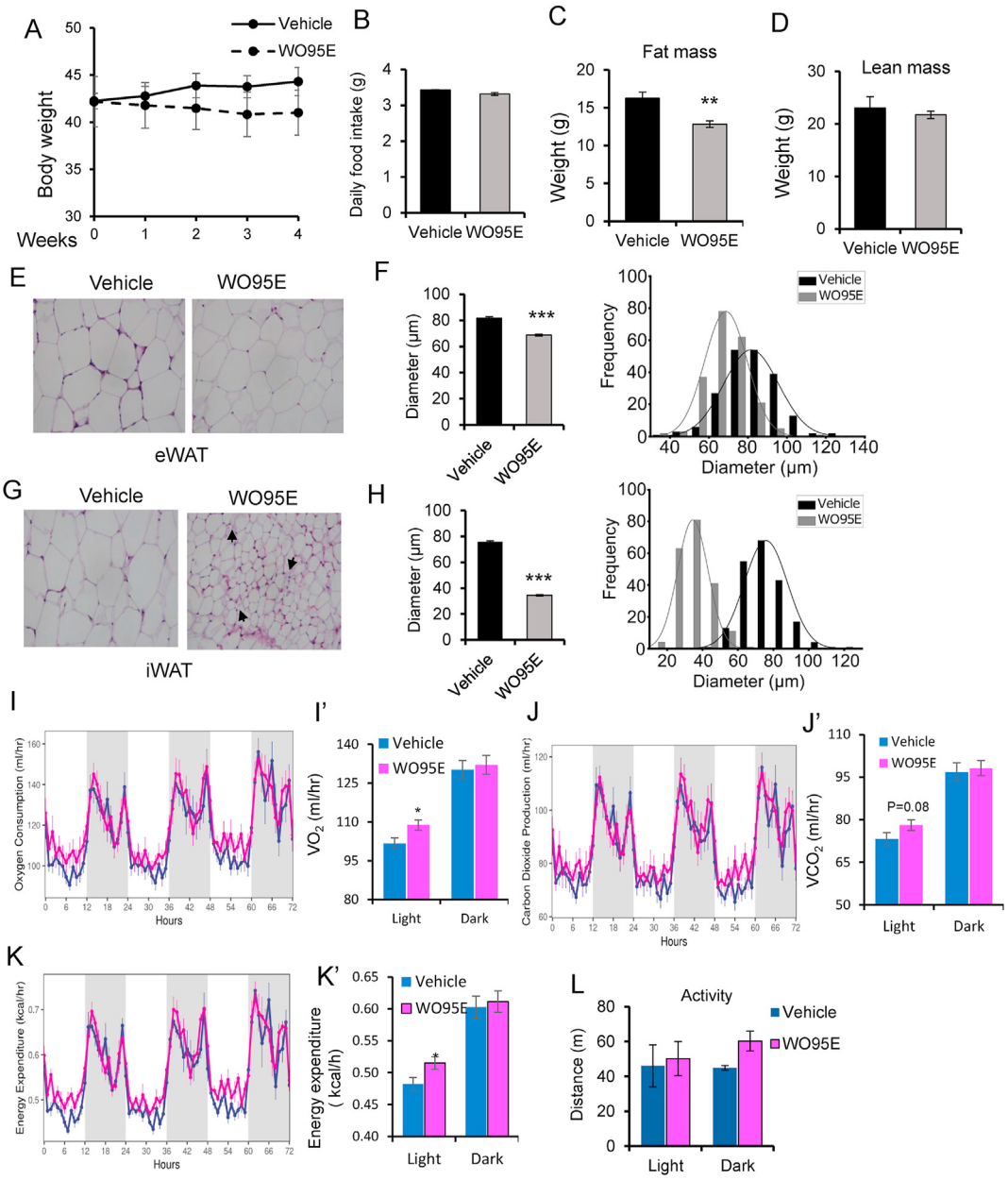

Figure 4: WO95E protects against obesity, decreases fat weight, and increases energy expenditure in DIO mice. A. Body weight of DIO mice treated with WO95E (n = 8) or vehicle (n = 7). B. Daily food intake, measured for three days during the 4th week of treatment. C. Fat mass. D. Lean mass. E-F. eWAT adipocytes. E. Representatives H&E staining of eWAT. F. Average diameter of adipocytes (μM)/field and size distribution. G-H. iWAT adipocytes. G. Representatives H&E staining of iWAT. H. Average diameter (μM)/field and size distribution. Arrows point to multilocular cells. I-L. Metabolic cage analysis after 4-week treatment. I—I'. Measurement of oxygen consumption levels. J—J'. Measurement of CO_2 production levels. K—K'. Energy expenditure levels. L. Distance of activity (m/mouse). Data are the mean ± SEM. *P < 0.05, **P < 0.01, and ***P < 0.001.

WO95E treatment reduced body weight during the period of 4-week treatment. This reduction was not due to the decrease in food intake, as we detected the same amount of daily food intake in mice between WO95E and vehicle treatments (Figure 4B). Body composition analysis using EchoMRI further revealed a significant decrease in the fat mass in WO95E-treated DIO mice (Figure 4C) with no noticeable change in lean mass (Figure 4D), suggesting that the body weight reduction is largely due to fat mass reduction. We next analyzed adipocytes in WAT sections and observed that adipocytes were significantly smaller with a lower average cell size in both eWAT (Figure 4E and F) and iWAT (Figure 4G and H) in WO95E-treated DIO mice than in vehicle-treated mice.

The finding that WO95E protects against HFD-induced obesity without altering food intake (Figure 4A and B) suggests an increase in energy expenditure. We therefore investigated energy expenditure in DIO mice treated with WO95E using indirect calorimetry. We observed that average oxygen consumption (VO_2) was higher in DIO mice treated with WO95E than with vehicle (Figure 4I—4I'). We similarly detected that average carbon dioxide production (VCO_2) was increased in WO95E-treated DIO mice but with a p value at 0.08 for daytime (Figure 4J—J'). WO95E treatment significantly heightened mean energy expenditure compared to vehicle treatment (Figure 4K—K'). In contrast, WO95E-treated DIO mice exhibited similar respiratory

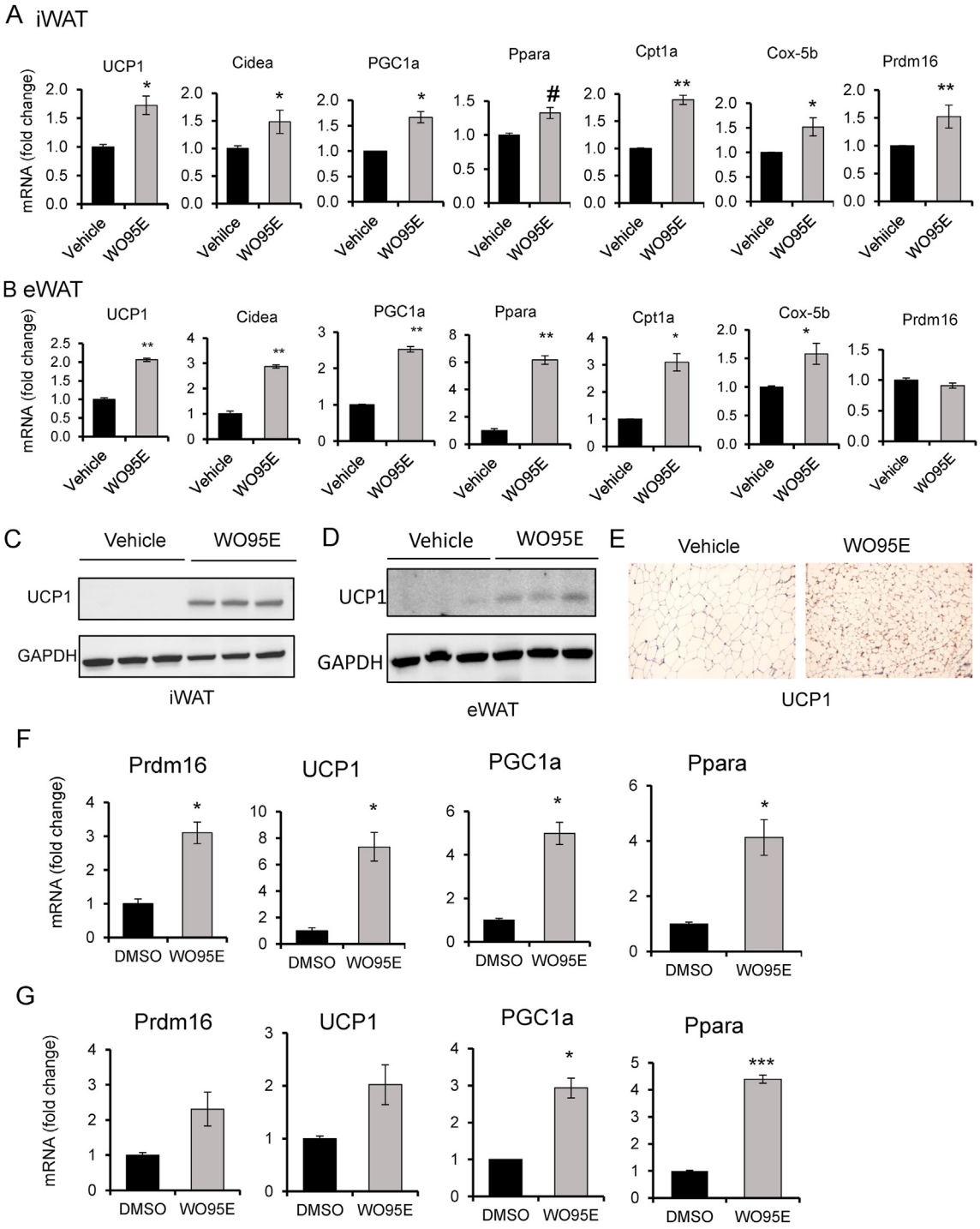

Figure 5: WO95E promotes WAT browning. A-B. mRNA levels of browning/thermogenic marker genes in iWAT (A) and in eWAT (B) from DIO mice treated with WO95E vs. vehicle. The results are expressed as fold change and are representative of 3 independent experiments. Data are expressed as mean ± SEM. *P < 0.05, **P < 0.01, and ***P < 0.001. C-D. Protein levels of UCP1 in iWAT (C) and eWAT (D) from DIO mice treated with WO95E vs. vehicle, assessed by western blotting. The data shown are representative of 3 independent experiments. E. Representative images of immunochemistry staining of UCP1 protein in iWAT from DIO mice treated with WO95E vs. vehicle. F-G. mRNA levels of browning/thermogenic marker genes in adipocytes differentiated from wild-type iWAT (F) and eWAT (G) treated with DMSO or WO95E. The results are expressed as fold change and are representative of 3 independent experiments. Data are expressed as mean ± SEM. *P < 0.05, **P < 0.01, and ***P < 0.001.

exchange ratio (RER) value as vehicle-treated DIO mice, suggesting that WO95E does not alter the relative contribution of carbohydrate and lipids to elicit an increase in energy expenditure (Figure S3). We also detected an upward trend in the overall activity of DIO mice treated with WO95E, but with the difference being statistically insignificant (Figure 4L).

3.5. Conversion of white to brown adipose tissue in WO95E-treated mice

Brown adipose tissue (BAT) is specialized for energy expenditure. BAT activation and brown remodeling of WAT increases energy expenditure [17]. We investigated whether WO95E increases overall energy expenditure by promoting the browning of WAT. We first examined the expression of genes that are involved in thermogenic and mitochondrial functions and enriched in BAT, including Prdm16, UCP1, Cidea, Ppara, CPT1a, Cox-5b, and PGC1α, in WAT. We detected significantly increased mRNA levels of Prdm16, Cidea, Ppara, CPT1a, UCP1, Cox5b, and PGC1α in the iWAT of DIO mice subjected to WO95E treatment compared to vehicle (Figure 5A). Similar results were obtained in the eWAT with the exception of Prdm16 mRNA (Figure 5B). We also observed increased mRNA expression levels of most of these genes in BAT tissues (Figure S4A), suggesting the prevention/reversal of "whitening" of high fat diet-induced BAT. Western blotting revealed a dramatic induction of UCP1 protein, a brown adipocyte marker, in both iWAT and eWAT (Figure 5C and D), and an increase in the level of UCP1 protein in BAT tissue (Figure S4B). Histochemical staining also showed that UCP1 was enhanced in the WAT from WO95E-treated DIO mice (Figure 5E). We frequently observed the occurrence of multilocular brown/beige adipocytes (multiple small lipids droplets, a hallmark of brown-like cells) in iWAT from DIO mice treated with WO95E (Figure 4G). Together, these results support the notion that WO95E induces white to brown/beige adipocyte conversion.

To investigate whether WO95E achieves the browning effects by directly acting on adipose tissues, we treated primary preadipocytes freshly isolated from iWAT with WO95E. WO95E significantly increased the expression levels of Prdm16, UCP1, PCG1α, and Ppara, genes involved in thermogenic/brown activities, but not in the adipogenic genes, in the iWAT adipocytes (Figure 5F and Figure S4C). Similar results were obtained in WO95E-treated primary preadipocytes isolated from eWAT (Figure 5G). These results show that WO95E acts directly on adipose tissues for the white to brown conversion.

3.6. WO95E ameliorates inflammation in adipose tissue

In obesity, there is significant accumulation of macrophages in the adipose tissue. It was proposed that the polarized recruitment/accumulation of pro-inflammatory M1 macrophages from the anti-inflammatory alternatively activated macrophages (M2) is critical for the development of systemic insulin resistance [18,19]. We interrogated whether WO95E could impact the adipose tissue inflammation. First, we measured the area of crown-like structures (CLS) in the subcutaneous and visceral fat depots. CLSs are characteristic elements that are formed upon the infiltration and recruitment of macrophages (marked by F4/80) around dead adipocytes in the adipose tissues [20]. As shown in Figure 6A—B', the areas of CLS were dramatically reduced in both iWAT and eWAT of DIO mice treated with WO95E relative to vehicle-treated mice. We investigated whether WO95E treatment affects the expression of genes involved in inflammation in the adipose tissue. We found that the mRNA levels of genes that encode pan-macrophage markers (CD68 and F4/80) were significantly decreased in the SVF portion of both inguinal (Figure 6C) and epididymal (Figure 6D) adipose tissues of DIO mice treated with WO95E compared to vehicle. WO95E also down-regulated the mRNA levels of genes that encode proinflammatory mediators [*TNFα*, *IL1b*, *IL-6*, and monocyte chemoattractant protein-1 (*mcp-1*), which are all enriched in M1 macrophages] in iWAT (Figure 6E) and in eWAT (Figure S5). In contrast, the mRNA levels of genes that encode the markers (IL4, IL10, and Mgll) for M2 macrophages were up-regulated or unchanged in the SVF portion of both inguinal and epididymal adipose tissues from WO95E-treated DIO mice (Figure 6F and Figure S6). These results indicate that WO95E lessens the adipose tissue inflammation in obesity.

3.7. WO95E improves hepatic steatosis in DIO mice

A common comorbidity of obesity and insulin resistance is nonalcoholic fatty liver disease (NAFLD) [21]. Given that WO95E improves systemic insulin in DIO mice and that PPARγ full agonist TZDs improve the condition of fatty liver [22], we investigated the potential effects of WO95E on liver steatosis in obesity. First, we examined the liver histology in haematoxylin and eosin-stained sections. We observed the presence of numerous lipid droplets in the liver, a hallmark of live steatosis, in the vehicle-treated DIO mice compared to that in the BL/6 mice (Figure 7A—B). WO95E treatment markedly reduced the number of the lipid droplets in the liver of DIO mice compared to vehicle treatment (Figure 7B—C). We next examined the expression of genes involved in lipogenesis in the liver of the WO95E- and vehicle-treated DIO mice and found that the lipogenic genes FASN, stearoly-coA desaturase-1 (*SCD-1*), and acetyl coA-carboxylase (*ACC*) were down-regulated in the liver of WO95E-treated DIO mice compared to vehicle-treated mice (Figure 7D). Because NAFLD is associated with an impaired suppression of hepatic glucose output [23], we assessed the expression of genes involved in gluconeogenesis, including glucose-6-phosphatase catalytic subunit (*G6PC*) and *PEPCK*. We found that the expression levels of PEPCK and G6PC in the liver from WO95E-treated DIO mice were also significantly decreased compared to that of vehicle-treated ones (Figure 7E).

3.8. WO95E has minimal TZD-associated side effects

PPARγ full agonist TZDs have been linked to multiple adverse side effects. We investigated whether as a partial PPARγ ligand that also inhibits its phosphorylation, WO95E is spared of the TZD-linked adverse side effects. Fluid retention, adiposity, and weight gain are among the most frequent side effects associated with TZD use [24]. However, WO95E did not cause weight gain and adiposity— instead decreased both the body weight and fat mass (Figure 4A and C). In addition, as shown in Figure 8A, while treatment with Rosi caused a significant reduction in packed-cell volume (PCV) that is indicative of hemodilution, the PCV was unchanged following WO95E treatment.

TZD use is associated with cardiac hypertrophy or dysfunction, which are partially attributable to fluid retention and weight gain [24]. We investigated the effect of WO95E on the heart weight and found that, unlike the TZD drug Rosi, which induces a significant increase in heart weight relative to vehicle, WO95E had no effect on weight gain in the heart (Figure 8B). We then assessed the expression of cardiac genes associated with heart failure or hypertrophy, such as myosin heavy chain β (β-Mhc, also Myh7) and natriuretic peptide B (Nppb) [4]. As expected, Rosi treatment increased the mRNA levels of *Myh7* (Figure 8C) and *Nppb* (Figure 8D) compared to vehicle treatment, observations that are consistent with previous findings [25]. In contrast, the mRNA levels of *Myh7* and *Nppb* were not significantly altered or even lowered in the hearts of DIO mice treated for WO95E (Figure 8C and D). TZD is also associated with a decrease in bone formation and bone mineral density and presents an increased risk for bone fracture [26]. As shown in Figure 8E—G, 4-week treatment of WO95E in DIO mice had no apparent effect on the mRNA levels of genes involved in bone formation, including osteocalcin (Bglap), osteopontin (SPP1) and ColA1, whereas Rosi treatment decreased their expression significantly.

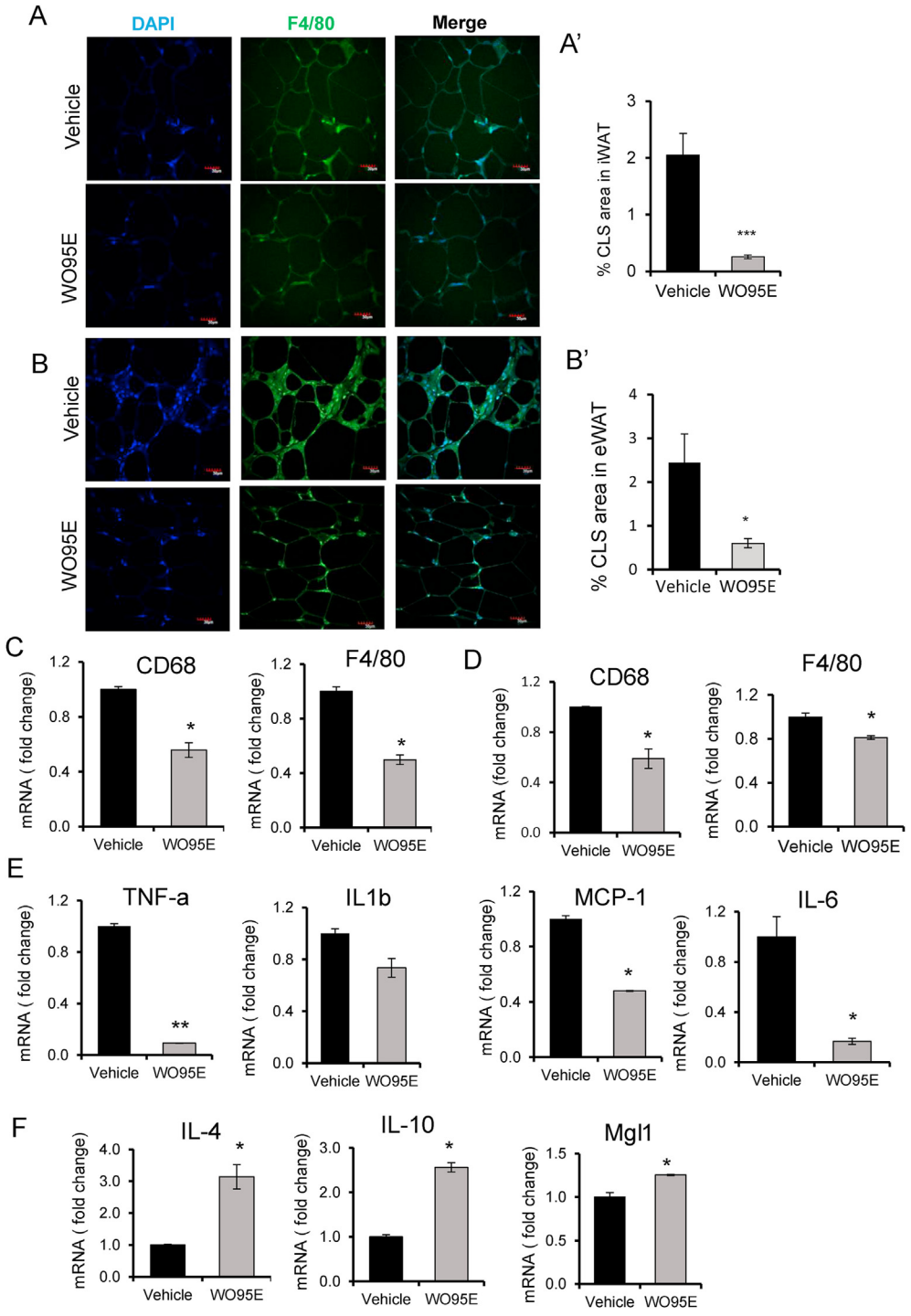

Figure 6: WO95E suppresses inflammation in adipose tissues in DIO mice. A—A'. Representative images of H.E. staining of iWAT from DIO mice treated with WO95E or vehicle (A). Quantification of percentage of CLS area in iWAT (A'). B—B'. Representative images of H.E. staining of eWAT from DIO mice treated with WO95E or vehicle (B). Quantification of percentage of CLS area in eWAT (B'). C—D. mRNA levels of genes as pan-macrophage markers in iWAT (C) and eWAT (D). E. mRNA levels of genes associated with M1 subtype in iWAT. F. mRNA levels of genes associated with M2 subtype in iWAT. The results are means of 3 replicate wells and are representative of 3 independent experiments for C—F. Data are expressed as mean ± SEM. *P < 0.05, **P < 0.01, and ***P < 0.001.

4. DISCUSSION

Obesity-associated insulin resistance is a core feature of type 2 diabetes (T2D) and other metabolic disorders. PPARγ full agonist TZD drugs were once widely used to treat T2D due to their potent effect on insulin sensitization [27]. However, the TZD drugs are associated with serious adverse effects, including weight gain, fluid retention, and congestive heart failure as full agonism is responsible for the activation of genes that are associated with these side effects; as a consequence, the prescription of TZD drugs has fallen tremendously recently.

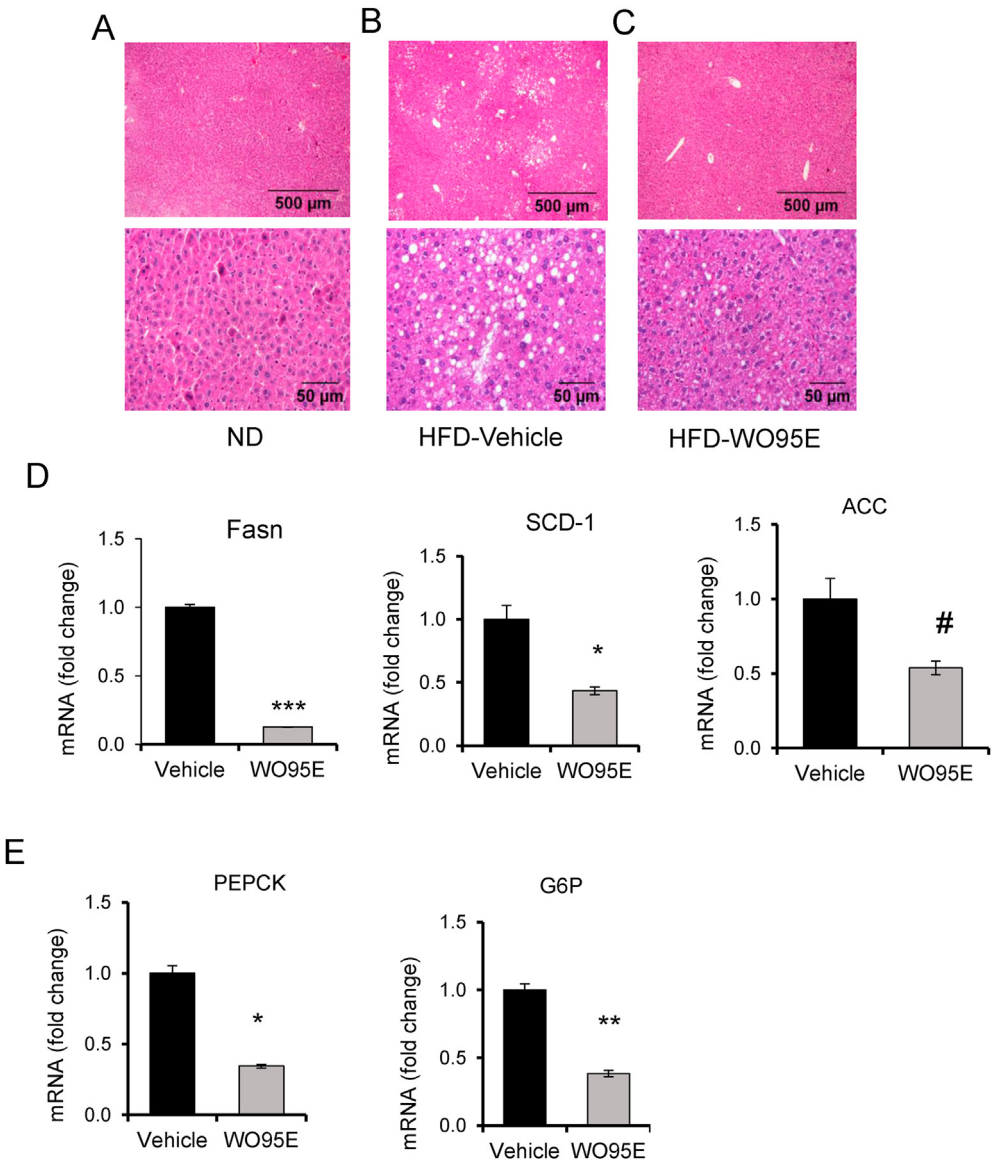

Figure 7: WO95E improves liver steatosis in DIO mice. A. Representative images of H.E. staining of liver slides from mice fed normal chow diet, or fed HFD treated with WO95E or vehicle. B. mRNA levels of lipogenic genes in livers from DIO mice treated with WO95E or vehicle. C. mRNA levels of gluconeogenic genes in livers from DIO mice treated with WO95E or vehicle. The results are means of 3 replicate wells and are representative of 3 independent experiments for B and C. Data are expressed as mean ± SEM. *P < 0.05, **P < 0.01, and ***P < 0.001.

Research focus has now been shifted to understand mechanisms that decouple the insulin sensitivity from TZD-associated side effects. Recent studies have shown that the insulin-sensitizing effect of TZD drugs is achieved through their inhibition of PPARγ pS273, which is independent on their classical full agonism. Several PPARγ ligands such as SR1664 and UHC1 have been shown to suppress PPARγ S273 phosphorylation, exert glucose-lowering activity while without the commonly observed side effects associated with TZDs. However, chemicals that bind to PPARγ with high affinity are still lacking.

In this study, we have developed a novel indole derivative WO95E that acts as a PPARγ partial agonist with a high binding affinity (IC_{50} ~11 nM). WO95E blocks PPARγ S273 phosphorylation both in vitro and in vivo. As expected, WO95E improves glucose disposal and insulin resistance in DIO mice. Blockage of PPARγ S273 phosphorylation is thought to decouple TZD-associated side effects from insulin sensitivity. Several side effects such as weight gain, adiposity, and fluid retention can occur within a short time after the administration of TZDs [5,28], but unlike the TZD drug Rosi which increases body weight, WO95E does not cause weight gain; instead, it reduces body weight (Figure 4A) and adiposity (Figure 4C and E—H). WO95E does not appear to cause Rosi-associated water retention, cardiac hypertrophy, or bone density-associated gene expression (Figure 8). Together, these results demonstrate that WO95E can improve insulin sensitization without the incurrence of adverse side effects.

One remarkable finding in this study is that WO95E promotes white-to-brown adipocyte conversion, as seen by an increase in adipocytes with multilocular appearance in the WAT of WO95E-treated mice (Figure 4G). In line with the known role of brown adipocytes in consuming energy reserves through nonshivering thermogenesis, we observed that WO95E treatment increases oxygen consumption, CO_2

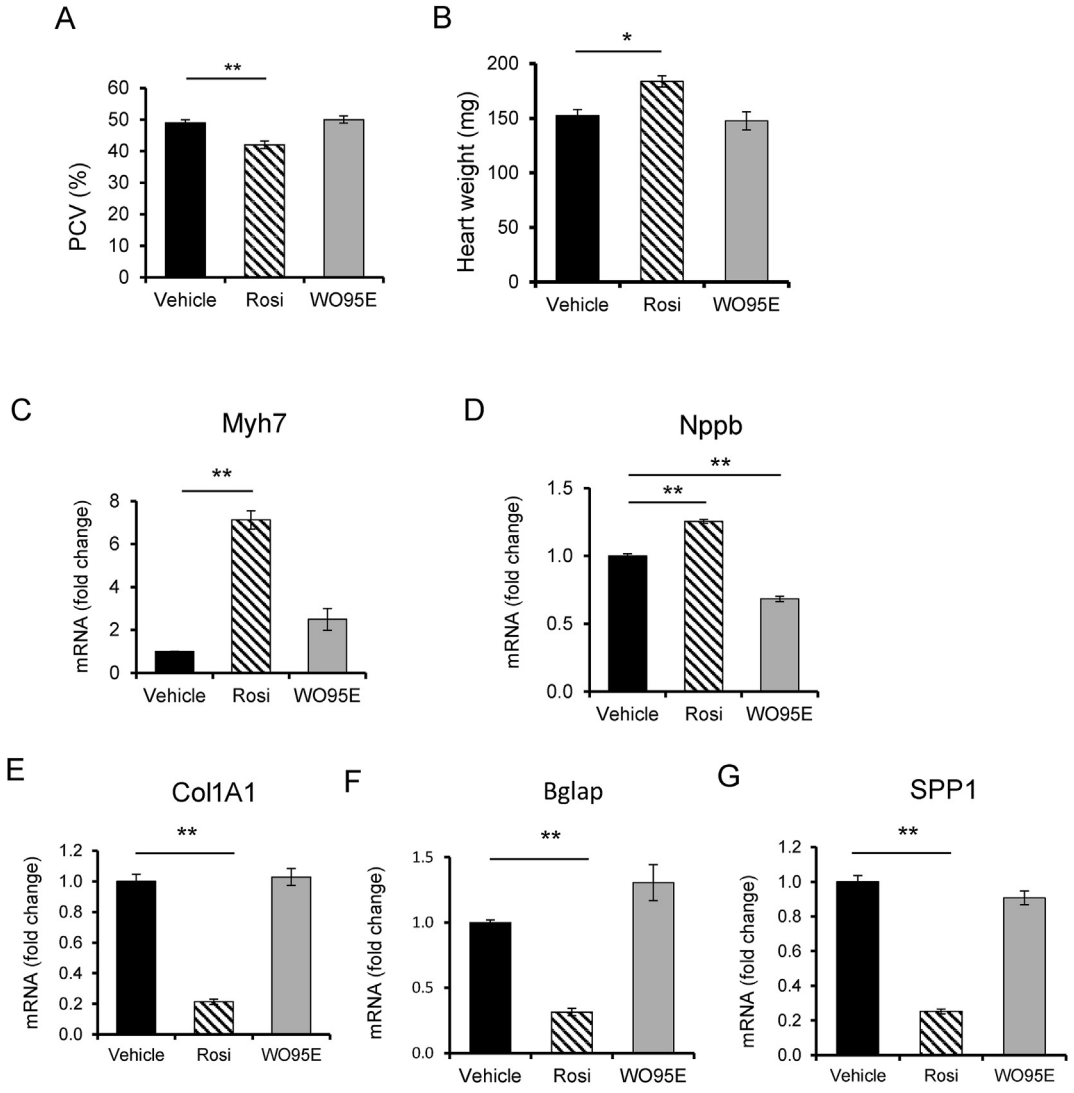

Figure 8: WO95E is devoid of common TZD-associated side effects. A. PCV measurement in DIO mice treated with WO95E (n = 8) or vehicle (n = 7). B. Heart weight of DIO mice treated with WO95E (n = 8) or vehicle (n = 7). C-D. mRNA levels of heart failure/hypertrophy associated genes Myh7 (C) and Nppb (D) in hearts from DIO mice treated with WO95E or vehicle. E-G. mRNA levels of bone density/formation-associated genes ColA1 (E), Bglap (F), and SPP1 (G) in bones from DIO mice treated with WO95E or vehicle. The results are means of 3 replicate wells and are representative of 3 independent experiments for B and C. Data are expressed as mean ± SEM. *P < 0.05, **P < 0.01, and ***P < 0.001.

production, and energy expenditure in DIO mice (Figure 4I—K). Consistently, genes involved in mitochondrial thermogenesis are up-regulated in WAT as well as BAT in WO95E-treated animals. Further experiments on isolated preadipocytes treated with WO95E indicate that WO95E acts directly on adipose tissues to promote the browning of WAT. PPARγ agonist TZD drugs have previously been shown to possess the ability to activate the brown remodeling of WAT [6,7,29,30]. Ohno et al. [7] further reported that only TZDs, but not non-TZD partial agonists tested, were capable of inducing the brown conversion of white adipocyte tissue, rendering the authors to conclude that the full PPARγ agonism is required for the browning. An alternative interpretation for these results is that the presence of TZD moiety in the tested full agonists may account for the positive effect on browning. Our findings that the novel non-TZD partial agonist WO95E of PPARγ promotes the browning of WAT indicate that neither TZD backbone nor full agonism is required for white-to-brown adipocyte conversion—instead we propose that WO95 likely induces browning in the same fashion as it improves insulin resistance through the inhibition of PPARγ S273 phosphorylation.

We observed that the effect of WO95E on insulin sensitivity is stronger than that of the recently reported PPARγ S273A knockin ($PPAR\gamma^{A/A}$ KI) model, which mimics the dephosphorylation [31]. The difference of the effect could lie on the nature of PPARγ activation. Like other nuclear receptors, PPARγ acts as a ligand-dependent transcription factor [32]. PPARγ functions as a heterodimer in association with co—regulator complex that binds to PPRE elements to either activate or repress the expression of its target genes. Once a ligand is present, the ligand binding to PPARγ stabilizes the structure of activation function 2 (AF-2) domain which acts as a binding site for coregulator proteins and facilitates its interaction with and recruitment of co-activators, thus leading to the expression of target genes. Conversely, in the absence of ligands, the heterodimers are more associated with co—repressor

complex which block gene transcription. In the case of PPARγ$^{A/A}$ KI mice, even though PPARγ S273A mimics the dephosphorylation, without potent exogenous ligands being present, PPARγ S273A proteins will not be expected to undergo ligand-dependent conformational changes and coregulator recruitment. Although several fatty acid derivatives have been reported to be the endogenous ligands of PPARγ, they do not appear to serve as biologically significant ligands due to their insufficient level in vivo [32]. For example, in obesity, the endogenous ligands do not appear to evoke a significant effect on insulin sensitivity improvement as opposed to exogenous ligands such as TZDs. On the other hand, W095E binding not only inhibits PPARγ S273 phosphorylation but also is expected to facilitate the recruitment of co-regulators. Although both PPARγ$^{A/A}$ KI and W095E have similar effect on S273 phosphorylation, the composition of coregulatory complexes would be different, which may explain the difference of the effects on insulin sensitivity or browning.

In conclusion, we developed a novel indole-based PPARγ partial agonist W095E that inhibits PPARγ phosphorylation and has potent insulin sensitizing effects without causing TZD-associated adverse effects. W095E promotes energy expenditure and protects against obesity by inducing the conversion of white fat to brown-like or beige fat as the first non-TZD partial agonist. These findings establish the potential for the development of novel therapeutics for the treatment of obesity and type 2 diabetes.

FUNDING

This work was supported by grants from the NIH (R01DK116017 and R01DK128848) and Oklahoma Center for Adult Stem Cell Research to W.W.

AUTHOR CONTRIBUTION

Wu D, Eeda V, Undi RB, Mann S, Stout M: Methodology, Investigation, Formal analysis, Visualization, Validation, Original draft preparation. **Lim H–Y:** Conceptualization, Supervision, Writing - Reviewing and Editing. **Wang W:** Conceptualization, Supervision, Writing - Reviewing and Editing, Funding acquisition.

ACKNOWLEDGMENTS

We thank the Diabetes CoBRE histology and Imaging (5P30GM122744) and Molecular Biology and Cytometry Research (P30CA225520) Cores at OUHSC for assistance on histology and microscopy use.

CONFLICT OF INTEREST

None declared.

APPENDIX A. SUPPLEMENTARY DATA

Supplementary data to this article can be found online at https://doi.org/10.1016/j.molmet.2021.101363.

REFERENCES

[1] Lazar, M.A., 2018. Reversing the curse on PPARγ. Journal of Clinical Investigation 128(6):2202–2204.

[2] Choi, J.H., Banks, A.S., Estall, J.L., Kajimura, S., Bostrom, P., Laznik, D., et al., 2010. Anti-diabetic drugs inhibit obesity-linked phosphorylation of PPARgamma by Cdk5. Nature 466(7305):451–456.

[3] Banks, A.S., McAllister, F.E., Camporez, J.P., Zushin, P.J., Jurczak, M.J., Laznik-Bogoslavski, D., et al., 2015. An ERK/Cdk5 axis controls the diabetogenic actions of PPARgamma. Nature 517(7534):391–395.

[4] Choi, J.H., Banks, A.S., Kamenecka, T.M., Busby, S.A., Chalmers, M.J., Kumar, N., et al., 2011. Antidiabetic actions of a non-agonist PPARgamma ligand blocking Cdk5-mediated phosphorylation. Nature 477(7365):477–481.

[5] Choi, S.-S., Kim, E.S., Koh, M., Lee, S.-J., Lim, D., Yang, Y.R., et al., 2014. A novel non-agonist peroxisome proliferator-activated receptor γ (PPARγ) ligand UHC1 blocks PPARγ phosphorylation by cyclin-dependent kinase 5 (CDK5) and improves insulin sensitivity. Journal of Biological Chemistry 289(38):26618–26629.

[6] Vernochet, C., Peres, S.B., Davis, K.E., McDonald, M.E., Qiang, L., Wang, H., et al., 2009. C/EBPalpha and the corepressors CtBP1 and CtBP2 regulate repression of select visceral white adipose genes during induction of the brown phenotype in white adipocytes by peroxisome proliferator-activated receptor gamma agonists. Molecular and Cellular Biology 29(17):4714–4728.

[7] Ohno, H., Shinoda, K., Spiegelman, B.M., Kajimura, S., 2012. PPARgamma agonists induce a white-to-brown fat conversion through stabilization of PRDM16 protein. Cell Metabolism 15(3):395–404.

[8] Soccio, R.E., Li, Z., Chen, E.R., Foong, Y.H., Benson, K.K., Dispirito, J.R., et al., 2017. Targeting PPARgamma in the epigenome rescues genetic metabolic defects in mice. Journal of Clinical Investigation 127(4):1451–1462.

[9] MacDougald, O.A., Lane, M.D., 1995. Transcriptional regulation of gene expression during adipocyte differentiation. Annual Review of Biochemistry 64(1):345–373.

[10] Aune, U.L., Ruiz, L., Kajimura, S., 2013. Isolation and differentiation of stromal vascular cells to beige/brite cells. Journal of Visualized Experiments(73):e50191.

[11] Mina, A.I., LeClair, R.A., LeClair, K.B., Cohen, D.E., Lantier, L., Banks, A.S., et al., 2018. A web-based analysis tool for indirect calorimetry experiments. Cell Metabolism 28(4):656–666.e1.

[12] Bae, H., Jang, J.Y., Choi, S.S., Lee, J.J., Kim, H., Jo, A., et al., 2016. Mechanistic elucidation guided by covalent inhibitors for the development of anti-diabetic PPARγ ligands. Chemical Science 7(8):5523–5529.

[13] Hughes, T.S., Giri, P.K., de Vera, I.M., Marciano, D.P., Kuruvilla, D.S., Shin, Y., et al., 2014. An alternate binding site for PPARγ ligands. Nature Communications 5:3571.

[14] Eeda, V., Wu, D., Lim, H.Y., Wang, W., 2019. Design, synthesis, and evaluation of potent novel peroxisome proliferator-activated receptor γ indole partial agonists. Bioorganic & Medicinal Chemistry Letters 29(22):126664.

[15] Bruning, J.B., Chalmers, M.J., Prasad, S., Busby, S.A., Kamenecka, T.M., He, Y., et al., 2007. Partial agonists activate PPARgamma using a helix 12 independent mechanism. Structure 15(10):1258–1271.

[16] Leesnitzer, L.M., Parks, D.J., Bledsoe, R.K., Cobb, J.E., Collins, J.L., Consler, T.G., et al., 2002. Functional consequences of cysteine modification in the ligand binding sites of peroxisome proliferator activated receptors by GW9662. Biochemistry 41(21):6640–6650.

[17] Kajimura, S., Spiegelman, B.M., Seale, P., 2015. Brown and beige fat: physiological roles beyond heat generation. Cell Metabolism 22(4):546–559.

[18] Reilly, S.M., Saltiel, A.R., 2017. Adapting to obesity with adipose tissue inflammation. Nature Reviews Endocrinology 13(11):633–643.

[19] Lumeng, C.N., Saltiel, A.R., 2011. Inflammatory links between obesity and metabolic disease. Journal of Clinical Investigation 121(6):2111–2117.

[20] Cinti, S., Mitchell, G., Barbatelli, G., Murano, I., Ceresi, E., Faloia, E., et al., 2005. Adipocyte death defines macrophage localization and function in adipose tissue of obese mice and humans. Journal of Lipid Research 46(11):2347–2355.

[21] Khan, R.S., Bril, F., Cusi, K., Newsome, P.N., 2019. Modulation of insulin resistance in nonalcoholic fatty liver disease. Hepatology 70(2):711–724.

[22] Ozturk, Z.A., Kadayifci, A., 2014. Insulin sensitizers for the treatment of nonalcoholic fatty liver disease. World Journal of Hepatology 6(4):199–206.

[23] Marchesini, G., Brizi, M., Bianchi, G., Tomassetti, S., Bugianesi, E., Lenzi, M., et al., 2001. Nonalcoholic fatty liver disease: a feature of the metabolic syndrome. Diabetes 50(8):1844—1850.

[24] Nesto, R.W., Bell, D., Bonow, R.O., Fonseca, V., Grundy, S.M., Horton, E.S., et al., 2004. Thiazolidinedione use, fluid retention, and congestive heart failure. The American Heart Association and American Diabetes Association 27(1):256—263.

[25] Chang, C.-S., Tsai, P.-J., Sung, J.-M., Chen, J.-Y., Ho, L.-C., Pandya, K., et al., 2014. Diuretics prevent thiazolidinedione-induced cardiac hypertrophy without compromising insulin-sensitizing effects in mice. American Journal Of Pathology 184(2):442—453.

[26] Kahn, S.E., Zinman, B., Lachin, J.M., Haffner, S.M., Herman, W.H., Holman, R.R., et al., 2008. Rosiglitazone-associated fractures in type 2 diabetes. A Diabetes Outcome Progression Trial (ADOPT) 31(5):845—851.

[27] Soccio, R.E., Chen, E.R., Lazar, M.A., 2014. Thiazolidinediones and the promise of insulin sensitization in type 2 diabetes. Cell Metabolism 20(4): 573—591.

[28] Nesto, R.W., Bell, D., Bonow, R.O., Fonseca, V., Grundy, S.M., Horton, E.S., et al., 2004. Thiazolidinedione use, fluid retention, and congestive heart failure: a consensus statement from the American Heart Association and American Diabetes Association. Diabetes Care 27(1):256—263.

[29] Petrovic, N., Walden, T.B., Shabalina, I.G., Timmons, J.A., Cannon, B., Nedergaard, J., 2010. Chronic peroxisome proliferator-activated receptor gamma (PPARgamma) activation of epididymally derived white adipocyte cultures reveals a population of thermogenically competent, UCP1-containing adipocytes molecularly distinct from classic brown adipocytes. Journal of Biological Chemistry 285(10):7153—7164.

[30] Tai, T.A., Jennermann, C., Brown, K.K., Oliver, B.B., MacGinnitie, M.A., Wilkison, W.O., et al., 1996. Activation of the nuclear receptor peroxisome proliferator-activated receptor gamma promotes brown adipocyte differentiation. Journal of Biological Chemistry 271(47):29909—29914.

[31] Hall, J.A., Ramachandran, D., Roh, H.C., DiSpirito, J.R., Belchior, T., Zushin, P.H., et al., 2020. Obesity-linked PPARγ S273 phosphorylation promotes insulin resistance through growth differentiation factor 3. Cell Metabolism 32(4):665—675.e6.

[32] Tontonoz, P., Spiegelman, B.M., 2008. Fat and beyond: the diverse biology of PPARgamma. Annual Review of Biochemistry 77:289—312.

